All-optical generation of deterministic squeezed Schrödinger-cat states

Zhucheng Zhang [1], Lei Shao,[1] Wangjun Lu [1,2] and Xiaoguang Wang[1,3,*]

[1]*Zhejiang Institute of Modern Physics, School of Physics, Zhejiang University, Hangzhou 310027, China*
[2]*Department of Maths and Physics, Hunan Institute of Engineering, Xiangtan 411104, China*
[3]*Graduate School of China Academy of Engineering Physics, Beijing 100193, China*

Quantum states are important resources and their preparations are essential prerequisites to all quantum technologies. However, they are extremely fragile due to the inevitable dissipations. Here the all-optical generation of a deterministic squeezed Schrödinger-cat state based on dissipation is proposed. Our system is based on the Fredkin-type interaction between three optical modes, one of which is subject to coherent two-photon driving and the others are coherent driving. We show that an effective degenerate three-wave-mixing process can be engineered in our system, which can cause the simultaneous loss of two photons, resulting in the generation of a deterministic squeezed Schrödinger-cat state. More importantly, by controlling the driving fields in our system, the two-photon loss can be adjustable, which can accelerate the generation of squeezed Schrödinger-cat states. In addition, we exploit the squeezed Schrödinger-cat states to estimate the phase in the optical interferometer and show that the quantum Fisher information about the phase can reach the Heisenberg limit in the limit of a large photon number. Meanwhile, it can have an order of magnitude factor improvement over the Heisenberg limit in the low-photon-number regime, which is very valuable for fragile systems that cannot withstand large photon fluxes. This work proposes an all-optical scheme to deterministically prepare the squeezed Schrödinger-cat state with high speed and can also be generalized to other physical platforms.

I. INTRODUCTION

The Schrödinger cat originally referred to a cat in a superposition of being dead versus alive, which was first introduced by Schrödinger to question the Copenhagen interpretation of quantum mechanics [1]. The cat being alive is macroscopically distinguishable from the cat being dead. In deference to Schrödinger's paradox of the cat, the superposition of the two coherent states with large and the same amplitude but a phase shift of π is called the Schrödinger-cat state [2,3]. According to the difference of the photon-number distributions, the Schrödinger-cat state can generally be divided into three cases [2,3]: An even coherent state (ECS) with an even number distribution, an odd coherent state (OCS) with an odd number distribution, and a Yurke-Stoler coherent state (YSCS) with a Poisson number distribution. Since the YSCS has a Poisson number distribution, it can be generated by a unitary time evolution with a Kerr-type nonlinearity [2,4–6]. The ECS and the OCS, however, cannot be prepared by a unitary time evolution. To generate the ECS and the OCS, one can exploit the interaction with other systems, such as an atom, followed by selective quantum measurements [2,7–12]. In addition, in stark contrast to dynamically transient preparation of the YSCS, the stable ECS and OCS can be deterministically generated by engineering a two-photon loss [13–23], which is very important for realistic applications. Schrödinger-cat states are not only fundamental studies of quantum mechanics, but also led to a boom in quantum information science.

Schrödinger-cat states have moved from basic research to actual quantum technologies, such as quantum computation [24–27] and quantum metrology [28–30]. It has been shown that Schrödinger-cat states have remarkable applications in error correction codes [31–34] and geometric quantum computation [35]. For quantum metrology based on optical interferometer, path-entangled Schrödinger-cat states can reach estimation precision with the Heisenberg limit (HL) for the linear phase and the super-Heisenberg limit for the nonlinear phase in the limit of a large photon number [29]. Unfortunately, for the phase estimation in the optical interferometer, it has been proved that the estimation precision depends mainly on the Mandel $\mathcal{Q}$ parameter of the quantum states and the correlations between the paths, i.e., path-entangled quantum states, can contribute at most a factor of 2 enhancement [36]. Meanwhile, in a practical situation, we must consider the capacity of the sample to withstand the photon fluxes, that is, we should focus on the measurements of the fragile systems in the low-photon-number regime.

To improve the estimation precision in the low-photon-number regime, many quantum states (including NOON states [37], squeezed entangled states [38], entangled even squeezed states [39], etc.) have been considered. However, the particularly promising approach is to squeeze a non-Gaussian state, and the squeezed Schrödinger-cat state is the one that has a large Mandel $\mathcal{Q}$ parameter, which can have a threefold improvement in the estimation over the optimal

---

*xgwang1208@zju.edu.cn

Gaussian state [38]. In addition, the squeezed Schrödinger-cat states also have been shown to have a significant role in quantum error correction [40]. For quantum technologies with squeezed Schrödinger-cat states, the preparation fidelity is crucial for realizing quantum advantage. There are some schemes to prepare the squeezed Schrödinger-cat states [41–44], but most of them rely on additional quantum measurements. Meanwhile, the preparation fidelities are only over 60% in experiments. There is still a lack of research to deterministically prepare the squeezed Schrödinger-cat states.

In this paper we propose an all-optical scheme to deterministically prepare the squeezed Schrödinger-cat states. In our scheme, based on the Fredkin-type interaction [45–47] between three optical modes, an effective degenerate three-wave-mixing process is engineered, which results in the generation of the two-photon loss in our system. Then the squeezed Schrödinger-cat states can be generated deterministically. The sizes of the squeezed Schrödinger-cat states and their squeezing amplitudes are well controllable by adjusting the driving fields of the optical modes. Moreover, the generation time of the squeezed Schrödinger-cat states can also be greatly shortened. With the generated squeezed Schrödinger-cat states in our scheme, we also estimate the linear phase in the optical interferometer. We find that the quantum Fisher information (QFI) about the phase can reach the HL in the limit of the large photon number; meanwhile, it can have an order of magnitude factor enhancement to the HL in the low-photon-number regime, which is valuable for the fragile systems to be measured.

This paper is organized as follows. In Sec. II we introduce the system model, discuss experimental feasibility, and then analyze the dynamic evolution. In Sec. III, by adjusting the driving fields of the optical modes in our system, we obtain squeezed Schrödinger-cat states with different sizes and squeezing amplitudes and analyze the robustness of the generated squeezed Schrödinger-cat states to the system loss. In Sec. IV we exploit the generated squeezed Schrödinger-cat states to estimate the phase of the optical interferometer and compare the QFI about the phase with the perfect squeezed Schrödinger-cat states. We summarize our conclusions in Sec. V.

II. MODEL AND HAMILTONIAN

As shown in Fig. 1(a), we consider an all-optical scheme to prepare squeezed Schrödinger-cat states based on the Fredkin-type interaction between three optical modes [45–47] represented by annihilation (creation) operators a ($a^\dagger$), b ($b^\dagger$), and c ($c^\dagger$) and their corresponding resonance frequencies ω_a, ω_b, and ω_c. The Fredkin-type interaction describes a conditional two-mode exchange interaction (here modes b and c) that depends on the number of photons in another mode (here mode a). Based on the Fredkin-type interaction, an all-optical platform to simulate an ultrastrong optomechanical coupling has been proposed [48]. In our scheme, the optical mode a is subject to a coherent two-photon driving and modes b and c are driven by a coherent driving field, with amplitudes Ω_i, frequencies ω_i, and phases ϕ_i ($i = 1, 2, 3$). In a rotating frame with respect to $U_1 = \exp\{i[\omega_1 a^\dagger a + \omega_3(b^\dagger b + c^\dagger c)]t\}$,

(a)

$ga^\dagger a$

b c

Fredkin-type interaction

(b)

$-0.20 \quad -0.08 \quad 0.05 \quad 0.18 \quad 0.30 \quad W$
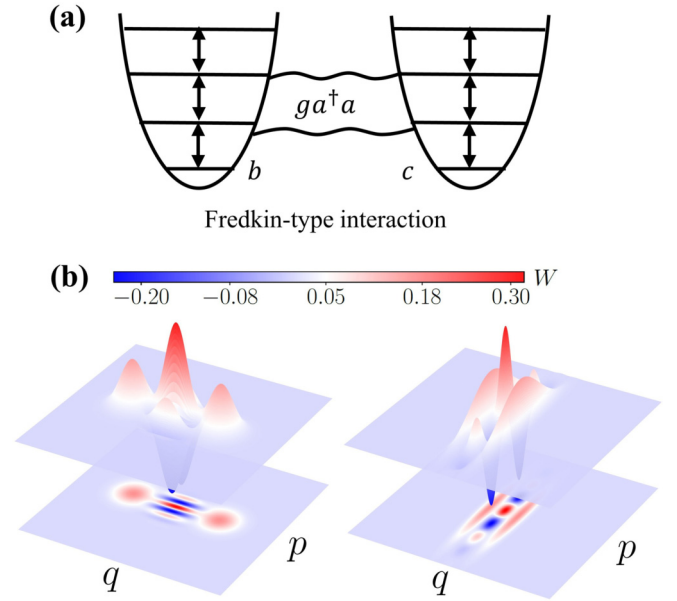
p

q

p

q

FIG. 1. (a) All-optical platform to prepare the squeezed Schrödinger-cat states based on the Fredkin-type interaction [45–47] between three optical modes (i.e., a, b, and c; g is the coupling strength). With the beam-splitter and the cross-Kerr interactions among these three optical modes, the Fredkin-type interaction can be constructed [45–48]. (b) Wigner function of the squeezed Schrödinger-cat states (here as squeezed even coherent states) in the position-momentum space (q, p). Here $q_0 = (\alpha + \alpha^*)/\sqrt{2}$ and $p_0 = (\alpha - \alpha^*)/i\sqrt{2}$ with the amplitude $\alpha = 2$ and the squeezing amplitude $r = 0$ for the left and $r = 1.1$ for the right. The two peaks in the Wigner function correspond to the dead cat and the alive cat in Schrödinger's paradox of the cat.

the system Hamiltonian can be written as ($\hbar = 1$)

$$\begin{aligned}
H = {} & \Delta_a a^\dagger a + \Delta_b b^\dagger b + \Delta_c c^\dagger c + ga^\dagger a(b^\dagger c + c^\dagger b) \\
& + \Omega_1(a^2 e^{-i\phi_1} + a^{\dagger 2} e^{i\phi_1}) \\
& + \Omega_2[be^{i(\omega_2-\omega_3)t}e^{-i\phi_2} + b^\dagger e^{-i(\omega_2-\omega_3)t}e^{i\phi_2}] \\
& + \Omega_3(ce^{-i\phi_3} + c^\dagger e^{i\phi_3}),
\end{aligned} \tag{1}$$

with detunings $\Delta_a = \omega_a - \omega_1$, $\Delta_b = \omega_b - \omega_3$, and $\Delta_c = \omega_c - \omega_3$. Here g describes the strength of the Fredkin-type interaction.

In our system, it is assumed that the three optical modes are coupled to the Markovian reservoir. Specifically, mode a is coupled to a squeezed-vacuum reservoir with a squeezing amplitude r_e and phase ϕ_e, and modes b and c are coupled to an individual thermal reservoir. The squeezed-vacuum reservoir can generally be realized by introducing an auxiliary mode generated by an optical parametric amplification [3,49]. For an optical mode, the thermal photon number in the thermal reservoir can be ignored safely and then the thermal reservoir can be viewed as a vacuum reservoir. Thus, the evolution of our system in an open environment can be governed by the master equation

$$\frac{d}{dt}\rho = -i[H, \rho] + \kappa_a \mathcal{L}(a, \rho) + \kappa_b \mathcal{L}'(b, \rho) + \kappa_c \mathcal{L}'(c, \rho), \tag{2}$$

with the dissipations caused by the system-environment coupling

$$\mathcal{L}(o, \rho) = (N_e + 1)\mathcal{D}[o]\rho + N_e\mathcal{D}[o^\dagger]\rho$$
$$- M_e\mathcal{G}[o]\rho - M_e^*\mathcal{G}[o^\dagger]\rho,$$
$$o = a, \qquad (3)$$

$$\mathcal{L}'(o, \rho) = \mathcal{D}[o]\rho, \quad o = b, c, \qquad (4)$$

where $N_e = \sinh^2(r_e)$ and $M_e = \sinh(r_e)\cosh(r_e)e^{i\phi_e}$ are the mean photon number and the two-photon correlation strength in the squeezing-vacuum reservoir, respectively. Here $\mathcal{D}[o]\rho = o\rho o^\dagger - (o^\dagger o\rho + \rho o^\dagger o)/2$, $\mathcal{G}[o]\rho = o\rho o - (oo\rho + \rho oo)/2$, and κ_o are the decay rates of the three optical modes.

There is a linear term of mode c in the Hamiltonian, i.e., $\Omega_3(ce^{-i\phi_3} + c^\dagger e^{i\phi_3})$, which can be removed by performing a displacement transformation on mode c with the displacement operator $D(\eta) = \exp(\eta c^\dagger - \eta^* c)$. Then the master equation in the displacement representation can be derived as (see Appendix A for details)

$$\frac{d}{dt}\rho_{\text{dis}} = -i[H_{\text{dis}}, \rho_{\text{dis}}] + \kappa_a\mathcal{L}(a, \rho_{\text{dis}}) + \kappa_b\mathcal{L}'(b, \rho_{\text{dis}})$$
$$+ \kappa_c\mathcal{L}'(c, \rho_{\text{dis}}), \qquad (5)$$

where the density operator in the displacement representation is $\rho_{\text{dis}} = D(\eta)\rho D^\dagger(\eta)$ and the Hamiltonian in the displacement representation becomes

$$H_{\text{dis}} = \Delta_a a^\dagger a + \Delta_b b^\dagger b + \Delta_c c^\dagger c - ga^\dagger a(b^\dagger\eta + b\eta^*)$$
$$+ ga^\dagger a(b^\dagger c + c^\dagger b) + \Omega_1(a^2 e^{-i\phi_1} + a^{\dagger 2}e^{i\phi_1})$$
$$+ \Omega_2[be^{i(\omega_2-\omega_3)t}e^{-i\phi_2} + b^\dagger e^{-i(\omega_2-\omega_3)t}e^{i\phi_2}], \qquad (6)$$

with the amplitude of the displacement operator $\dot\eta = -(i\Delta_c + \kappa_c/2)\eta + i\Omega_3 e^{i\phi_3}$ and its steady value $\eta_s = \Omega_3 e^{i\phi_3}/(\Delta_c - i\kappa_c/2)$. Herein we focus on the steady-state region and η_s can be a real number by adjusting the phase ϕ_3 of the driving field. From Eq. (6) we can find that there is an optomechanical-like interaction $g\eta_s a^\dagger a(b^\dagger + b)$ with an adjustable coupling $g\eta_s$. By controlling the amplitude Ω_3 of the driving field, an ultrastrong optomechanical-like interaction can be obtained [48], which can be equivalent to a Kerr-like interaction and help to dynamically produce the YSCS [4,5]. However, we focus on preparing other types of (squeezed) Schrödinger-cat states, which will be shown in the following sections to have better applications than (squeezed) YSCS.

In our system, mode a is subject to a coherent two-photon driving and then we can remove the quadratic term in the Hamiltonian of Eq. (6) by carrying out a squeezing transformation on mode a with the squeeze operator $S(\zeta) = \exp[(\zeta a^{\dagger 2} - \zeta^* a^2)/2]$. The squeeze parameter $\zeta = r\exp(i\phi_1)$ with amplitude r and phase ϕ_1. The master equation in the squeezing representation can be derived as (see Appendix B for details)

$$\frac{d}{dt}\rho_{\text{sq}} = -i[H_{\text{sq}}, \rho_{\text{sq}}] + \kappa_a\mathcal{L}(a, \rho_{\text{sq}}) + \kappa_b\mathcal{L}'(b, \rho_{\text{sq}})$$
$$+ \kappa_c\mathcal{L}'(c, \rho_{\text{sq}}), \qquad (7)$$

with

$$\mathcal{L}(o, \rho_{\text{sq}}) = (N_{\text{eff}} + 1)\mathcal{D}[o]\rho_{\text{sq}} + N_{\text{eff}}\mathcal{D}[o^\dagger]\rho_{\text{sq}}$$
$$- M_{\text{eff}}\mathcal{G}[o]\rho_{\text{sq}} - M_{\text{eff}}^*\mathcal{G}[o^\dagger]\rho_{\text{sq}},$$
$$o = a, \qquad (8)$$

$$\mathcal{L}'(o, \rho_{\text{sq}}) = \mathcal{D}[o]\rho_{\text{sq}}, \quad o = b, c, \qquad (9)$$

where the density operator in the squeezing representation is $\rho_{\text{sq}} = S(\zeta)D(\eta)\rho D^\dagger(\eta)S^\dagger(\zeta)$ and the mean photon number and the two-photon correlation strength become (setting $\phi_1 = 0$)

$$N_{\text{eff}} = \sinh^2(r)\cosh^2(r_e) + \cosh^2(r)\sinh^2(r_e)$$
$$+ \frac{1}{2}\cos(\phi_e)\sinh(2r)\sinh(2r_e), \qquad (10)$$

$$M_{\text{eff}} = [\cosh(r)\cosh(r_e) + e^{-i\phi_e}\sinh(r)\sinh(r_e)]$$
$$\times [\sinh(r)\cosh(r_e) + e^{i\phi_e}\cosh(r)\sinh(r_e)], \qquad (11)$$

from which one can see that the mean photon number and the two-photon correlation strength can be suppressed completely (i.e., $N_{\text{eff}}, M_{\text{eff}} = 0$) when we reasonably adjust the amplitude and phase of the squeezed-vacuum reservoir under the parameter conditions [49]: $r_e = r$ and $\phi_e = \pm n\pi$ $(n = 1, 3, 5, \ldots)$. In this case, the squeezed-vacuum reservoir with the same squeezing amplitude as mode a becomes a vacuum reservoir under phase matching, which plays a very important role in suppressing the influence of noise on the system, such as enhanced nonlinear interaction [49], optical nonreciprocity [50], and state preparation [12,51–53]. In addition, the Hamiltonian in the squeezing representation can be derived as (dropping constant terms)

$$H_{\text{sq}} = \omega_{sa}a^\dagger a + \Delta_b b^\dagger b + \Delta_c c^\dagger c + \frac{g_p\eta_s}{2}(a^2 b^\dagger + a^{\dagger 2}b)$$
$$+ \Omega_2[be^{i(\omega_2-\omega_3)t}e^{-i\phi_2} + b^\dagger e^{-i(\omega_2-\omega_3)t}e^{i\phi_2}] + H_{\text{nr}}, \qquad (12)$$

$$H_{\text{nr}} = \left[\frac{g_p\eta_s}{2}a^2 b - \frac{g_p}{2}(a^2 b^\dagger c + a^2 c^\dagger b)\right.$$
$$\left. - (g_s a^\dagger a + g\sinh^2 r)(b\eta_s - bc^\dagger)\right] + \text{H.c.}, \qquad (13)$$

with the transformed frequency of mode a, $\omega_{sa} = \Delta_a/\cosh(2r)$, the couplings $g_s = g\cosh(2r)$ and $g_p = g\sinh(2r)$, and the squeeze amplitude $r = \frac{1}{4}\ln[(\Delta_a + 2\Omega_1)/(\Delta_a - 2\Omega_1)]$. The value of the squeeze amplitude r can be adjustable by controlling the amplitude and detuning of the driving field. In the interaction picture with $U_2 = \exp[i(\omega_{sa}a^\dagger a + \Delta_b b^\dagger b + \Delta_c c^\dagger c)t]$, the Hamiltonian can be rewritten as

$$H_I = \frac{g_p\eta_s}{2}(a^2 b^\dagger + a^{\dagger 2}b) + \Omega_2(be^{-i\phi_2} + b^\dagger e^{i\phi_2}) + H_{\text{nr}}', \qquad (14)$$

$$H_{\text{nr}}' = \left[\frac{g_p\eta_s}{2}a^2 be^{-2i\Delta_b t} - \frac{g_p}{2}(a^2 b^\dagger c e^{-i\Delta_c t}\right.$$
$$+ a^2 c^\dagger b e^{-i(2\Delta_b-\Delta_c)t}) - (g_s a^\dagger a + g\sinh^2 r)(b\eta_s e^{-i\Delta_b t}$$
$$\left. - bc^\dagger e^{-i(\Delta_b-\Delta_c)t})\right] + \text{H.c.}, \qquad (15)$$

where we have assumed that $2\omega_{sa} = \Delta_b$ and $\omega_2 - \omega_3 = \Delta_b$. Under the parameter conditions $2\Delta_b \gg$

$(g_p \eta_s n_a \sqrt{n_b}/2, 2g_s \eta_s n_a \sqrt{n_b}, 2g \eta_s \sinh^2 r \sqrt{n_b})$, $|\Delta_b - \Delta_c| \gg$ $(g_s n_a \sqrt{n_b n_c}, g \sinh^2 r \sqrt{n_b n_c})$, and $|\Delta_b - \Delta_c \pm 2\omega_{sa}| \gg$ $g_p n_a \sqrt{n_b n_c}/2$, with $n_o (o = a, b, c)$ the dominant excitation numbers in mode o, the Hamiltonian in Eq. (15) becomes the term that oscillates with high frequency and can be safely ignored under the rotating-wave approximation (RWA). Then the total Hamiltonian in the interaction picture can be reduced to

$$H_I = G(a^2 b^\dagger + a^{\dagger 2} b) + \Omega_2 (b e^{-i\phi_2} + b^\dagger e^{i\phi_2}), \quad (16)$$

with the coupling strength $G = g_p \eta_s / 2$ between modes a and b. From Eq. (16) one can see that it is a Hamiltonian that describes the degenerate three-wave-mixing process of modes a and b, where a photon of mode b is absorbed from (emitted into) the driving field with amplitude Ω_2 and two photons of mode a are created (annihilated) simultaneously.

The Fredkin-type interaction is an optical process, which was mainly used to design logic gates [45,46]. In our work, we obtain the degenerate three-wave-mixing process from the driven all-optical system with the Fredkin-type interaction under the RWA. Realizing the Fredkin-type interaction is the key to the experimental realization of our all-optical scheme for obtaining the degenerate three-wave-mixing process. It has been suggested and analyzed that with the beam-splitter and cross-Kerr interactions among these three optical modes, the Fredkin-type interaction can be obtained and has been realized in experiments [45–48]. In addition, the validity of the RWA is manifested in our numerical simulation. As shown in the following sections, we will focus on the total Hamiltonian in Eq. (14) and the reduced Hamiltonian in Eq. (16) for analytical solution and numerical simulation [54,55] and we will show that a deterministic squeezed Schrödinger-cat state can be prepared based on the Fredkin-type interaction.

III. DETERMINISTIC GENERATION OF SQUEEZED SCHRÖDINGER-CAT STATES

A. Squeezed Schrödinger-cat states without single-photon loss

First, we assume that the decay rate of mode b is large enough, i.e., $\kappa_b \gg \kappa_a$, so that the decay rate of mode a can be neglected safely. In this case, mode b can be eliminated adiabatically and then the master equation of the system with the Hamiltonian in Eq. (16) becomes [13,14]

$$\frac{d}{dt}\rho_a = -i[H_{\text{eff}}, \rho_a] + \Gamma_a \mathcal{L}'(a^2, \rho_a), \quad (17)$$

where the effective Hamiltonian is $H_{\text{eff}} = iJ(a^2 - a^{\dagger 2})$ with the effective coupling $J = 2\Omega_2 e^{i\phi_2} G/\kappa_b$ describing the rates of simultaneous decay and excitation of two photons, respectively, ρ_a is the reduced density operator of mode a, and $\Gamma_a = 4G^2/\kappa_b$ is the effective two-photon decay rate. It has been proved analytically that the master equation (17) has a steady state for mode a, while, the steady state only depends on its initial excited number [13,14]. Specifically, for mode a initially in an even Fock state, its steady state is an ECS with even number distribution, i.e.,

$$|\psi_a\rangle = \mathcal{N}_e^{-1/2}(|\alpha\rangle + |-\alpha\rangle), \quad (18)$$

with the normalization coefficient $\mathcal{N}_e = 2[1 + \exp(-2|\alpha|^2)]$ and the amplitude $\alpha = \sqrt{-\Omega_2 e^{i\phi_2}/G}$. For mode a initially in an odd Fock state, it is an OCS with odd number distribution, i.e.,

$$|\psi_a\rangle = \mathcal{N}_o^{-1/2}(|\alpha\rangle - |-\alpha\rangle), \quad (19)$$

with the normalization coefficient $\mathcal{N}_o = 2[1 - \exp(-2|\alpha|^2)]$. For a generic initial state of mode a, its steady state will be a mixture of the ECS and the OCS.

In the derivation of the Hamiltonian above, one can find that four unitary transformations (with operators U_2, S, D, and U_1) have been made, so the state of mode a in the laboratory framework should be

$$|\psi_a\rangle_{\text{la}} = U_1^\dagger D^\dagger(\eta) S^\dagger(\zeta) U_2^\dagger |\psi_a\rangle$$
$$= \exp(-i\omega_1 a^\dagger a t) S^\dagger(\zeta)|\psi_a(\alpha')\rangle, \quad (20)$$

where $|\psi_a(\alpha')\rangle$ is still a Schrödinger-cat state with a modified amplitude $\alpha' = \alpha \exp(-i\omega_{sa}t)$. Meanwhile, the term $\exp(-i\omega_1 a^\dagger a t)$ only causes the state to rotate in the phase space and does not influence the properties of the state, such as the photon-number distribution and the average value of an observable. That is to say, in the laboratory framework, the state of mode a is a steady squeezed Schrödinger-cat state in our system. Note that this is different from the squeezing of mode a. In the following sections, for the sake of convenience, we will consider the state of mode a in the laboratory framework as $|\psi_a\rangle_{\text{la}} = S^\dagger(\zeta)|\psi_a(\alpha)\rangle$ and α as a real number.

In addition, according to Eqs. (16) and (17), one can also find that both the two-photon decay rate Γ_a and the coupling J are closely related to the coupling G that depends on the strength g of the Fredkin-type interaction. That is to say, the Fredkin-type interaction leads to the two-photon loss of mode a in our system, which makes mode a in the squeezed Schrödinger-cat state in the laboratory framework.

To see the quantum features of the generated squeezed Schrödinger-cat states, we now calculate the Wigner function analytically. The Wigner function is a phase-space quasiprobability distribution [3,56], which is defined in the position and momentum space (q, p) as

$$W(q, p) = \frac{1}{2\pi} \int_{-\infty}^{+\infty} dx \left\langle q - \frac{x}{2} \left| \rho_{\text{la}} \right| q + \frac{x}{2} \right\rangle e^{ipx}, \quad (21)$$

where $\rho_{\text{la}} = |\psi_a\rangle_{\text{la}}\langle\psi_a|$. For the squeezed even coherent state (SECS), the Wigner function is derived as

$$W(q, p) = W_1 + W_2 + W_{\text{in}}, \quad (22)$$

where

$$W_1 = \frac{\exp[-(e^{-r}p - p_0)^2 - (e^r q - q_0)^2]}{2\pi(1 + e^{-p_0^2 - q_0^2})}, \quad (23)$$

$$W_2 = \frac{\exp[-(e^{-r}p + p_0)^2 - (e^r q + q_0)^2]}{2\pi(1 + e^{-p_0^2 - q_0^2})}, \quad (24)$$

$$W_{\text{in}} = \frac{\exp(-e^{-2r}p^2 - e^{2r}q^2)}{\pi(1 + e^{-p_0^2 - q_0^2})} \cos[2(e^{-r}pq_0 - e^r p_0 q)], \quad (25)$$

with $q_0 = (\alpha + \alpha^*)/\sqrt{2}$ and $p_0 = (\alpha - \alpha^*)/i\sqrt{2}$. Similarly, one can calculate the Wigner function of the squeezed odd coherent state (SOCS) according to its definition. From
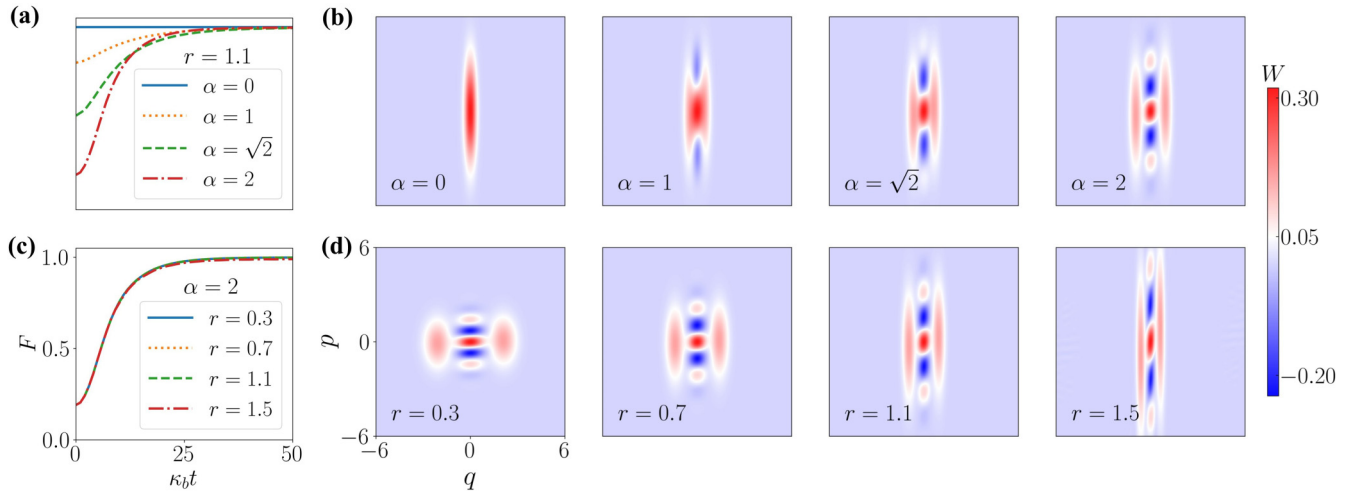
FIG. 2. (a) and (c) Time evolution of the fidelity F between the actual state ρ_{app} generated by our system and the exact squeezed Schrödinger-cat state ρ_{exa}, with different cat sizes α and squeezed amplitudes r. (b) and (d) Plots of Wigner function at steady state with (b) fixed squeezed amplitude $r = 1.1$ and different cat sizes α and with (d) fixed cat size $\alpha = 2$ and different squeezed amplitudes r. In the laboratory framework, modes a, b, and c are initially in the squeezed vacuum state, vacuum state, and coherent state, respectively. The parameters are set as $\Delta_a = 100\kappa_b$, $g = 10^{-5}\Delta_a$, $\Delta_c = 11\Delta_b$, $G = 0.1\kappa_b$, $\kappa_c = \kappa_b$, and $\kappa_a = 0$. Other parameters can be obtained from their relations in the text.

Eqs. (23)–(25) one can see that the Wigner function exhibits two squeezed peaks at the position-momentum space ($q = \pm e^{-r}q_0$, $p = \pm e^r p_0$). Meanwhile, there are quantum interference and coherence effects between the two peaks, displaying the superposition of both amplitudes and showing rapid oscillations. As shown in Fig. 1(b), we plot the Wigner function of the SECS with squeeze amplitudes $r = 0$ and 1.1 based on Eq. (22). Similar to Schrödinger's paradox of the cat, the two peaks in the Wigner function correspond to the "dead cat" and the "alive cat.". One can see that the Wigner functions show negative values, indicating the nonclassical feature of the squeezed Schrödinger-cat state. Moreover, the optical mode a is squeezed on the position q at the expense of expanding in its momentum p.

Above we analyzed the deterministic generation of Schrödinger-cat states (i.e., squeezed Schrödinger-cat states in the laboratory framework) with the Hamiltonian in Eq. (16). We now use the total Hamiltonian in Eq. (14) to confirm the effectiveness of our all-optical platform to generate the squeezed Schrödinger-cat states. We define the fidelity F between the actual state ρ_{app} generated by our system and the exact, i.e., perfect, squeezed Schrödinger-cat state ρ_{exa} as

$$F = \mathrm{Tr}\left(\sqrt{\sqrt{\rho_{\mathrm{exa}}}\,\rho_{\mathrm{app}}\,\sqrt{\rho_{\mathrm{exa}}}}\right). \qquad (26)$$

When the fidelity F approaches 1, it means that the state generated by our system is the same as the perfect state. As shown in Fig. 2, we plot the time evolution of the fidelity F with different cat sizes α and squeezed amplitudes r, as well as the corresponding Wigner functions at steady state. One can see that the optical mode a is steered into a stable squeezed cat state with high fidelity even though there is a term H'_{nr} that makes the Wigner functions in these plots look tilted. Meanwhile, the cat size and the squeezed amplitude have good adjustability by controlling the driving fields in our system. In an actual experimental system, however, the decay rate of

mode a should be considered. In other words, the lifetime of the generated squeezed Schrödinger-cat states will be limited by the single-photon loss, so the effective two-photon decay rate Γ_a should be enhanced to make mode a able to reach its target state with high speed and high fidelity. From Eq. (17) we can see that the two-photon decay rate Γ_a is parabola dependent on the coupling G. That is to say, the coupling G should be large. Unlike the general schemes, our system has the advantage of enhancing the coupling G by adjusting the parameters of the driving field, i.e., the steady-state value η_s. As shown in Fig. 3(a), by adjusting the steady-state value η_s, the coupling G is linearly enhanced so that the two-photon decay rate Γ_a can be increased parabolically. Meanwhile, from Fig. 3(b) we can see that with a larger value of η_s (or coupling G), the optical mode a can reach the steady squeezed Schrödinger-cat state with higher speed (see the solid curve). Otherwise it will take a longer time to evolve to the steady
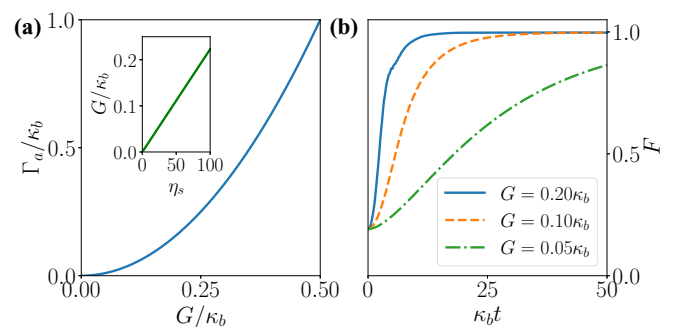

FIG. 3. (a) Effective two-photon decay rate Γ_a plotted as a function of coupling G. The inset shows the change of the coupling G with the parameter η_s of the driving field. (b) Evolution of the fidelity F with cat size $\alpha = 2$, squeeze amplitude $r = 1.1$, and different couplings $G(0.20\kappa_b, 0.10\kappa_b, 0.05\kappa_b)$. The other parameters are the same as those in Fig. 2.
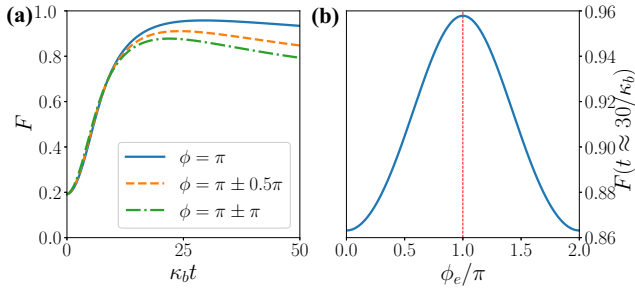
FIG. 4. (a) Evolution of the fidelity under the single-photon loss with different phases ϕ_e of the squeezed vacuum reservoir. (b) Fidelity at time $t \approx 30/\kappa_b$ as a function of the phase of the squeezed vacuum reservoir. The cat size $\alpha = 2$, squeeze amplitude $r = 1.1$, decay rate $\kappa_a = 10^{-3}\kappa_b$, and other parameters are the same as those in Fig. 2.

state (see the dot-dashed curve), which is undoubtedly detrimental to practical applications. Thus, with our all-optical system, parameter adjustable steady squeezed Schrödinger-cat states with high fidelity and speed can be obtained, which is advantageous in an actual situation.

B. Squeezed Schrödinger-cat states with single-photon loss

So far, we have not considered the decay rate κ_a, i.e., the single-photon loss, of the optical mode a and assumed the perfect phase matching of its squeezed-vacuum reservoir. The decay rate of the optical mode a will limit the lifetime of the generated squeezed Schrödinger-cat states. Meanwhile, the noise induced by the deviation of the phase ϕ_e in the squeezed-vacuum reservoir will also destroy the fidelity of the state. In this section we analyze the evolution of mode a under these imperfect factors.

As shown in Fig. 4, we plot the dependence of the fidelity F on the deviation of the phase ϕ_e under the single-photon loss, using the Hamiltonian (16). From Fig. 4(a) we can see that under the single-photon loss, the value of fidelity has a maximum value (about 0.958) at time $t \approx 30/\kappa_b$ when the phase matching is met. When there is a deviation of the phase, this maximum value at time $t \approx 30/\kappa_b$ decreases. Specifically, we plot the dependence of the fidelity $F(t \approx 30/\kappa_b)$ on the phase ϕ_e, as shown in Fig. 4(b). One can clearly see that the best fidelity occurs in the vicinity of the phase matching, i.e., $\phi_e = \pi$, and the deviation of the phase will decrease the value of fidelity. In experiments, light with a squeezing bandwidth up to GHz (MHz) in the optical (microwave) domain has been realized [57,58]. Thus, the squeezed-vacuum reservoir with this phase matching will have a very important role in suppressing the influence of noise on the system.

Then we simulate the long-time evolution of mode a under its single-photon loss with the total Hamiltonian. As shown in Fig. 5(a) (see the solid curve), we plot the time evolution of the fidelity F in the system under the single-photon loss of mode a. From the curve one can see that in an open system with a modest single-photon loss, mode a can be prepared to the squeezed Schrödinger-cat state with good fidelity. Then the fidelity decreases gradually and stays at a stable value in the end. We plot the Wigner function of mode a at different times as shown in Fig. 5(b). One can clearly see that with

the time evolution, the quantum interference and coherence effects between the two squeezed peaks disappear gradually. Moreover, the negative values of the Wigner function also disappear, which are in sharp contrast to Fig. 2. Finally, the two squeezed peaks remain in the plot of the Wigner function. Actually, one can see that under the single-photon loss, there will be an additional term, i.e., $\kappa_a \mathcal{L}'(a, \rho_a)$, in Eq. (17). Then, due to the simultaneous existence of single-photon and two-photon losses of mode a, mode a will be in a mixture of (approximately) two squeezed coherent states in the end after decaying out the coherence [13,14].

We also analyze the evolution of mode a with the two-photon loss turned off [i.e., $G = 0$ by adjusting the driving field; see Fig. 3(a)] after it evolves to a squeezed Schrödinger-cat state with good fidelity. In this case, mode a is only subjected to single-photon loss. Under single-photon loss, the density operator (here the SECS) of mode a will decay during the evolution and can be written as [59]

$$
\begin{aligned}
\rho_{\mathrm{doc}} = {}& N_e^{-1} S^\dagger \{ |\alpha e^{-\kappa_a t/2}\rangle \langle \alpha e^{-\kappa_a t/2}| + |-\alpha e^{-\kappa_a t/2}\rangle \langle -\alpha e^{-\kappa_a t/2}| \\
& + \exp[-2\alpha^2(1 - e^{-\kappa_a t})][|\alpha e^{-\kappa_a t/2}\rangle \langle -\alpha e^{-\kappa_a t/2}| \\
& + |-\alpha e^{-\kappa_a t/2}\rangle \langle \alpha e^{-\kappa_a t/2}|]\} S,
\end{aligned}
\tag{27}
$$

where the decay of the diagonal term is accompanied by energy loss, while the decay of the nondiagonal term is accompanied by the attenuation of coherence (i.e., decoherence). After a long time evolution with single-photon loss, the coherence of the generated squeezed Schrödinger-cat states and the energy of the system will disappear, so mode a will evolve into a squeezed vacuum state in the end. The lifetime of the squeezed Schrödinger-cat state can be approximated as $\tau = 1/2|\alpha|^2 \kappa_a$ according to the above equation [59]. As shown in Fig. 5(a) (see the dashed curve), we plot the evolution of the fidelity F in the system with only single-photon loss of mode a when it is evolved to the squeezed Schrödinger-cat state with good fidelity. From the curve one can see that the value of fidelity decreases monotonically and approaches its initial value, that is, mode a evolves to a squeezed vacuum state. Moreover, we also plot the Wigner function at the same times as in Fig. 5(b), as shown in Fig. 5(c). One can see that the difference between them is that the two squeezed peaks of the Wigner function decay into one squeezed peak in the end.

In the experiment, in order to quickly prepare squeezed Schrödinger-cat states and significantly prolong their lifetimes, we must enhance the effective two-photon loss Γ_a of mode a and choose a small decay rate κ_a of mode a. For a modest decay rate of the optical mode $\kappa_a \sim 10^5$ Hz [60], the lifetime of the state will be the order of microseconds. However, with a smaller decay rate, the lifetime of the state will be further increased. For example, with an extreme cavity decay rate (∼0.2 Hz), Schrödinger-cat states of the order of milliseconds have been prepared in an experiment [9]. In addition, due to the extremely weak spin relaxation, long-lived atomic Schrödinger-cat states of about 3 s have also been predicted in theory by engineering the two-atom decay [23]. That is to say, reducing the corresponding decay rate as much as possible will be the key to generate the quantum states in experiments.
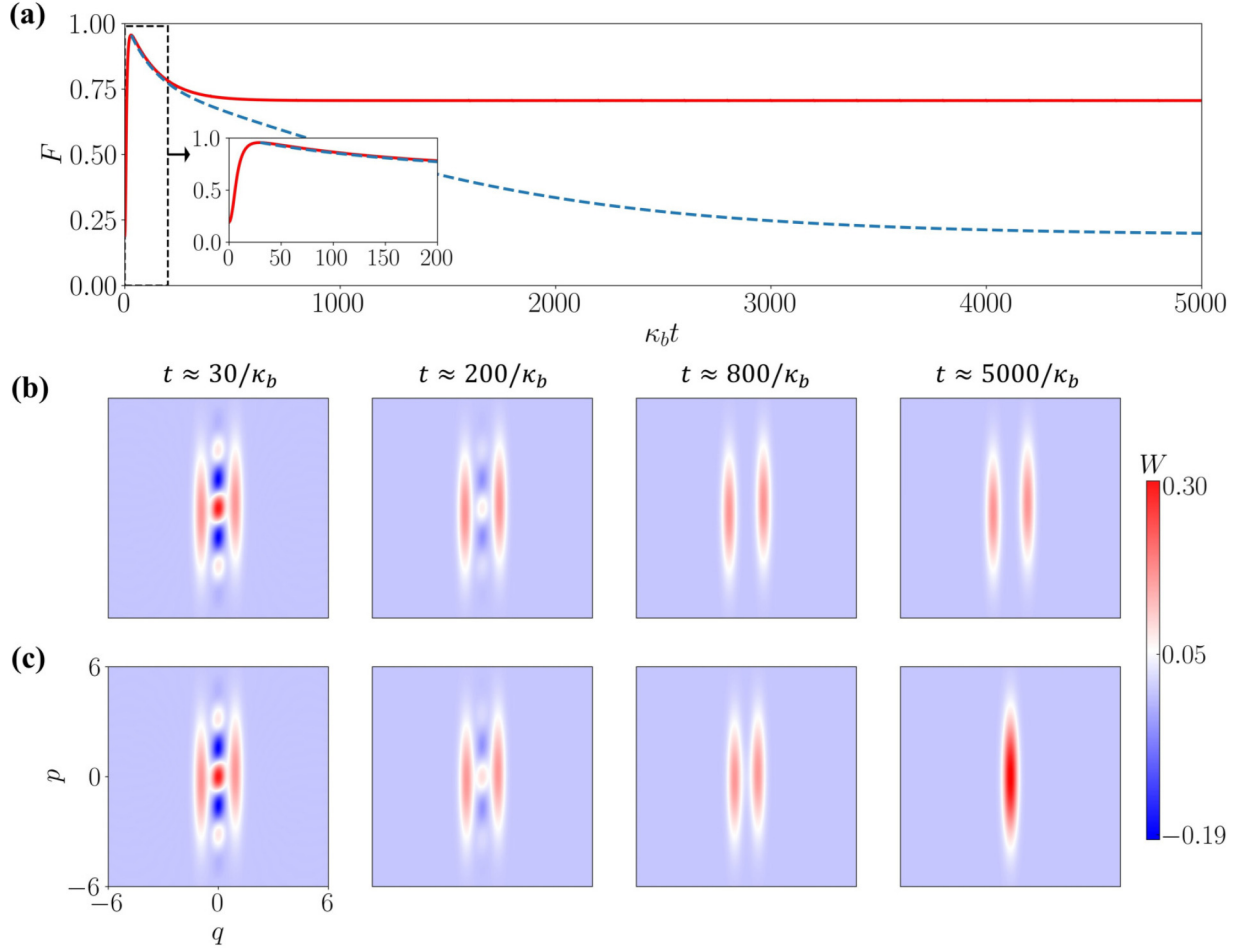
FIG. 5. (a) Time evolution of the fidelity F in the system with simultaneous single-photon and two-photon losses of mode a, i.e., solid curve, and with only the single-photon loss of mode a, i.e., dashed cure. (b) and (c) Plots of the Wigner function of mode a at different times ($t \approx 30/\kappa_b, 200/\kappa_b, 800/\kappa_b, 5000/\kappa_b$), corresponding to the solid and dashed curves in (a), respectively. The other parameters are the same as those in Fig. 2 except for $\alpha = 2$, $r = 1.1$, and $\kappa_a = 10^{-3}\kappa_b$.

IV. PHASE ESTIMATION WITH SQUEEZED SCHRÖDINGER-CAT STATES

Above we have shown that deterministic squeezed Schrödinger-cat states (i.e., SECSs, SOCSs, and their mixture) with high fidelity can be prepared in our all-optical platform by engineering two-photon loss. The light field in a squeezed Schrödinger-cat state can be applied to a variety of quantum technologies, such as quantum computation and quantum metrology. As an example, in this section, we exploit the squeezed Schrödinger-cat states generated by our system to estimate the phase in the optical interferometer and compare the QFI with those using the perfect squeezed Schrödinger-cat states. First, we estimate the phase based on the perfect squeezed Schrödinger-cat states. As shown in Fig. 6, there are two linear phase shifters that contain an unknown relative phase φ_1-φ_2 between the arms of the interferometer. The phase information will be imprinted on the initial quantum state in the input of the interferometer by the unitary evolution, i.e.,

$$|\Psi\rangle = U|\Psi_0\rangle, \tag{28}$$

where the unitary operator $U = \exp[i(\varphi_1 a_1^\dagger a_1 + \varphi_2 a_2^\dagger a_2)]$, with $a_{1,2}$ ($a_{1,2}^\dagger$) representing annihilation (creation) operators in arms 1 and 2, and $|\Psi_0\rangle = |\psi_1\rangle \otimes |\psi_2\rangle$ is the input state of the interferometer, with $|\psi_i\rangle$ ($i = 1, 2$) the perfect squeezed Schrödinger-cat states. Here we focus on the relative phase between the two arms and then for a path-symmetric initial state, the evolution operator U can be reduced to [61] $U = \exp(i\phi_- O_-)$, with $\varphi_- = \varphi_1 - \varphi_2$ and $O_- = (a_1^\dagger a_1 - a_2^\dagger a_2)/2$. For the unitary evolution of the initial state $|\Psi_0\rangle$, the QFI can be defined as [62–64]

$$\mathcal{F} = 4\langle\Psi_0|\Delta^2\mathcal{H}|\Psi_0\rangle, \tag{29}$$

where $\mathcal{H} = i(\partial_{\phi_-}U^\dagger)U$ and $\Delta^2\mathcal{H} = (\mathcal{H} - \langle\mathcal{H}\rangle)^2$. For the unbiased estimation, the bound of uncertainty of phase estimation is given by the quantum Cramér-Rao inequality, i.e., $\delta\phi_- \geqslant 1/\sqrt{F}$. When the QFI value is larger, it means that the phase can be evaluated more accurately. With the expression of the operator U, one can calculate the QFI as

$$\mathcal{F} = 2[\text{Var}_{\Psi_0}(a_i^\dagger a_i) - \text{Cov}_{\Psi_0}(a_1^\dagger a_1, a_2^\dagger a_2)], \quad i = 1 \text{ or } 2, \tag{30}$$
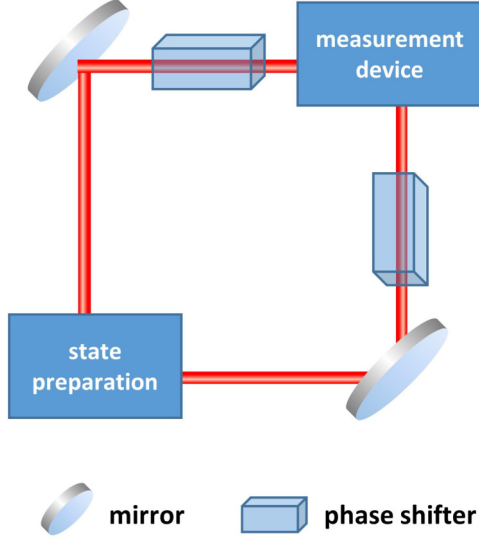
FIG. 6. Optical interferometer model used for the estimation of the phase. A prepared quantum state is sent into the interferometer, which contains an unknown relative phase φ_1-φ_2 generated by two linear phase shifters between its two arms. The phase information will be imprinted on the initial quantum state and be measured at the output ports.

where $\mathrm{Var}_{\Psi_0}(\bullet)$ and $\mathrm{Cov}_{\Psi_0}(\bullet)$ are the variance and the covariance in the state $|\Psi_0\rangle$, respectively. From Eq. (30) one can find that the value of the QFI only depends on the properties of the initial input state. As the initial state considered here is separable, we have $\mathrm{Cov}_{\Psi_0}(a_1^\dagger a_1, a_2^\dagger a_2) = 0$ and the QFI is reduced to the variance of the photon-number operator $a_i^\dagger a_i$.

Based on Eq. (30), we can calculate the expression of the QFI analytically for the perfect squeezed Schrödinger-cat states. Specifically, for the SECS, the QFI and the total average photon number N of the two arms are

$$\mathcal{F} = \sinh^2(2r) - 2\alpha^2 \mathrm{sech}(\alpha^2)\sinh(4r - \alpha^2)$$
$$+ 2\alpha^4 \cosh^2(2r)\mathrm{sech}^2(\alpha^2), \tag{31}$$

$$N = 2[\sinh^2(r) - \alpha^2 \mathrm{sech}(\alpha^2)\sinh(2r - \alpha^2)], \tag{32}$$

respectively. If the squeeze amplitude $r = 0$ (i.e., the ECS), they are reduced to $\mathcal{F} = 2\alpha^4 \mathrm{sech}^2(\alpha^2) + N$ and $N = 2\alpha^2 \tanh(\alpha^2)$, respectively. One can find that even if in the low-photon-number regime the QFI can beat the value of the standard quantum limit (SQL), i.e., $\mathcal{F} \sim N$, but its scaling can only reach the SQL in the limit of the large photon number. For the SOCS one has

$$\mathcal{F} = \sinh^2(2r) + 2\alpha^2 \mathrm{csch}(\alpha^2)\cosh(4r - \alpha^2)$$
$$- 2\alpha^4 \cosh^2(2r)\mathrm{csch}^2(\alpha^2), \tag{33}$$

$$N = 2[\sinh^2(r) + \alpha^2 \mathrm{csch}(\alpha^2)\cosh(2r - \alpha^2)]. \tag{34}$$

If the squeeze amplitude $r = 0$, i.e., the OCS, they are reduced to $\mathcal{F} = -2\alpha^4 \mathrm{csch}^2(\alpha^2) + N$ and $N = 2\alpha^2 \coth^2(\alpha^2)$, respectively. One can also find that in the limit of the large photon number the scaling of the QFI can reach the SQL, but it is inferior to the SQL in the low-photon-number regime. For
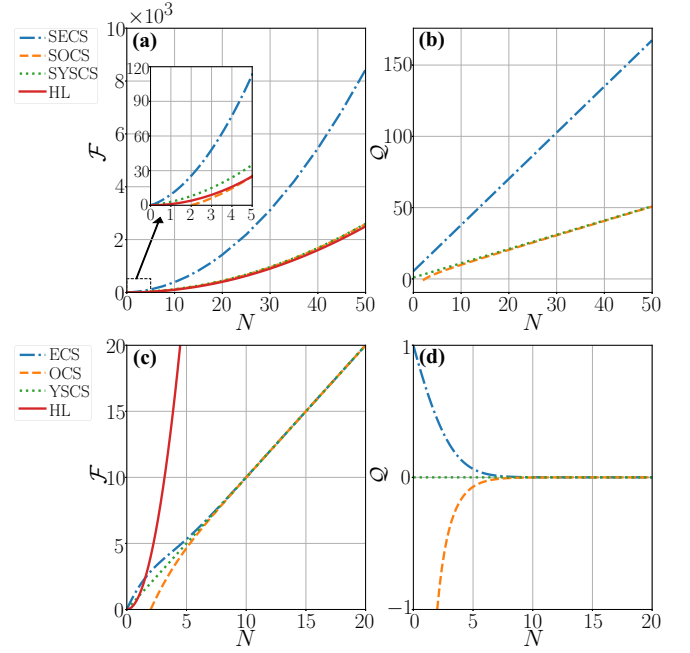

FIG. 7. (a) and (c) Quantum Fisher information (QFI) $\mathcal{F}$ plotted as a function of the average photon number N with different initial states, i.e., (a) squeezed even coherent state, squeezed odd coherent state, and squeezed Yurke-Stoler coherent state and (c) even coherent state, odd coherent state, and Yurke-Stoler coherent state. (b) and (d) Mandel parameter $\mathcal{Q}$ of the Schrödinger-cat states with and without squeezing plotted as a function of the average photon number N. Here HL represents the Heisenberg limit N^2. Note that the average photon numbers of the SOCS and the OCS are greater than or equal to 2, i.e., $N \geqslant 2$, due to their photon-number distributions.

comparison, we also calculate the case of the squeezed Yurke-Stoler coherent state (SYSCS), i.e, $|\psi\rangle = ^\dagger(r)[(\frac{1+i}{2})|\alpha\rangle + (\frac{1-i}{2})|-\alpha\rangle]$. The QFI and the average photon number become

$$\mathcal{F} = \sinh^2(2r) + 2e^{-4r}\alpha^2, \tag{35}$$

$$N = 2[\sinh^2(r) + \alpha^2 e^{-2r}]. \tag{36}$$

Similarly, when the squeeze amplitude $r = 0$ (i.e., YSCS), they are reduced to $\mathcal{F} = N$ and $N = 2\alpha^2$, respectively. One can clearly find that with the YSCS, the scaling of the QFI is only the SQL. From the expressions of the QFI using the squeezed Schrödinger-cat states, one can see that, compared with the one without squeezing, there are two parameters, i.e., r and α, that can be chosen to increase the value of the QFI. To see the scaling of this QFI, one can optimize the two parameters to maximize the QFI for a fixed average photon number. As shown in Fig. 7(a), we plot the QFI using the above three squeezed Schrödinger-cat states by numerically optimizing r and α with each fixed average photon number. From the curves one can see that the value of the QFI using the SECS is better than those using the SOCS and the SYSCS. Specifically, in the case of the large photon number, the values of the QFI using these three states are all higher than the value of the HL (corresponding to N^2), especially the SECS. In the case of the low photon number, however, the SOCS is lower than the HL [see the inset of Fig. 7(a)]. To see the scaling of

the QFI using these three types of squeezed Schrödinger-cat states in the limit of a large photon number, we numerically fit the relation of the QFI with the average photon number. For the SECS,

$$\mathcal{F} \approx 6.42N + 3.24N^2; \tag{37}$$

for the SOCS,

$$\mathcal{F} \approx -4.40 - 3.01N^{1/2} + 2.28N + N^2; \tag{38}$$

and for the SYSCS,

$$\mathcal{F} \approx 2N + N^2. \tag{39}$$

From the above equations, one can find that in the limit of a large photon number, the scaling of the QFI with these states is all the HL. Moreover, in the case of a low photon number, the QFI using the SECS has significant advantages in estimating the phase of the optical interferometer due to an order of magnitude factor improvement over the value of the HL, which is very important for fragile systems that cannot withstand large photon fluxes, such as spin ensembles [65], atoms [66], molecules [67], and biological systems [68]. In Fig. 7(c) we also plot the QFI for the ECS, the OCS, and the YSCS with different average photon numbers. Compared with Fig. 6(a), the scaling of the QFI with these states is only the SQL in the limit of a large number of photons. Thus, one can see the importance of squeezing the Schrödinger-cat states.

One can understand this squeezing-enhanced phase estimation as follows. As pointed out in Ref. [36], the QFI of Eq. (30) can be rewritten as

$$\mathcal{F} = N(1 + \mathcal{Q})(1 - \mathcal{J}), \tag{40}$$

where the Mandel parameter of mode a_i has the form $\mathcal{Q} = [\mathrm{Var}_{\Psi_0}(a_i^\dagger a_i) - \langle a_i^\dagger a_i \rangle]/\langle a_i^\dagger a_i \rangle$ and $\mathcal{J} = \mathrm{Cov}_{\Psi_0}(a_1^\dagger a_1, a_2^\dagger a_2)/\mathrm{Var}_{\Psi_0}(a_i^\dagger a_i)$ ranges from -1 to 1. For the input states considered here, the value of $\mathcal{J}$ is zero. So the Mandel parameter for the pure and separable initial states can be written as

$$\mathcal{Q} = \frac{\mathcal{F}}{N} - 1. \tag{41}$$

Then we can get the expressions of the above squeezed Schrödinger-cat states according to the fitting formulas (37)–(39). Specifically, for the SECS

$$\mathcal{Q} \approx 5.42 + 3.24N, \tag{42}$$

for the SOCS

$$\mathcal{Q} \approx -4.40N^{-1} - 3.01N^{-1/2} + 1.28 + N, \tag{43}$$

and for the SYSCS

$$\mathcal{Q} \approx 1 + N. \tag{44}$$

In addition, one can also get the versions without squeezing. As shown in Figs. 7(b) and 7(d), the Mandel parameter of the Schrödinger-cat states with and without squeezing is plotted as a function of the average photon number. One can find that the Mandel parameters of the squeezed Schrödinger-cat states are proportional to the average photon number, except for the SOCS with the low photon number [see Fig. 7(b)], which can contribute to bringing their QFI values to the HL in the limit of a large photon number. However, for the Mandel parameter of
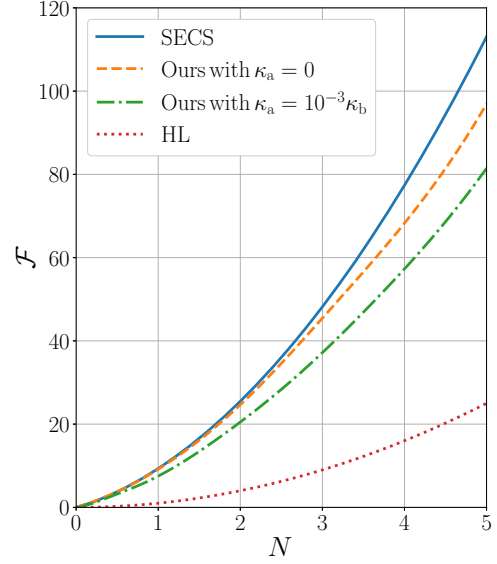

FIG. 8. Quantum Fisher information $\mathcal{F}$ plotted as a function of the average photon number N with the perfect squeezed even coherent state and the SECS generated by our system. Meanwhile, for the SECS generated by our system, we also consider the effect of the single-photon loss on the QFI. The other parameters are the same as those in Fig. 2.

the Schrödinger-cat states without squeezing [see Fig. 7(d)], one can clearly find that with the increase of the average photon number, the Mandel parameters all go to zero, whereas the YSCS remains zero. This causes their QFI values only to approach the SQL, which is in stark contrast to those of the corresponding squeezing Schrödinger-cat states.

From the above discussion we can conclude that the phase evaluation precision using the SECS is the best among the three squeezed Schrödinger-cat states. Now we estimate the phase based on the SECS generated by our all-optical system. For the case without the single-photon loss, i.e., $\kappa_a = 0$, we have shown that the squeezed Schrödinger-cat states with high fidelity can be prepared in our system (see Fig. 2). Then, according to Eq. (30), we numerically simulate the QFI in the low-photon-number regime, as shown in Fig. 8. We can see that due to the high fidelity of the squeezed Schrödinger-cat state generated by our system, the QFI values are in good agreement with the perfect one in the low-photon-number regime. When considering the effect of the single-photon loss, we also numerically calculate the QFI for the squeezed Schrödinger-cat states. In this case, the squeezed Schrödinger-cat states generated by our system will be a mixed state (see Fig. 5). For the mixed state, the QFI can be defined as [62–64]

$$\mathcal{F} = \sum_{i=1}^{M} \frac{(\partial_\theta p_{\mathrm{in},i})^2}{p_{\mathrm{in},i}} + \sum_{i=1}^{M} 4 p_{\mathrm{in},i} \langle \psi_{\mathrm{in},i} | \mathcal{H}^2 | \psi_{\mathrm{in},i} \rangle$$
$$- \sum_{i,j=1}^{M} \frac{8 p_{\mathrm{in},i} p_{\mathrm{in},j}}{p_{\mathrm{in},i} + p_{\mathrm{in},j}} |\langle \psi_{\mathrm{in},i} | \mathcal{H} | \psi_{\mathrm{in},j} \rangle|^2, \tag{45}$$

where $p_{\mathrm{in},i}$ and $|\psi_{\mathrm{in},i}\rangle$ are the ith eigenvalue and eigenstate of the density matrix ρ_0 of the input mixed state, respectively. Based on the QFI of the mixed state, we obtain its evolution

with the average photon number, as shown in Fig. 8. Due to the effect of the single-photon loss, we can see that compared with the case without the single-photon loss, the QFI values decrease for each fixed photon number, but they are far more than the value of the HL (N^2) in the low-photon-number regime.

V. CONCLUSION

We have proposed an all-optical platform based on the Fredkin-type interaction to deterministically generate the squeezed Schrödinger-cat states with high speed and high fidelity. We obtained the analytical expression of the Wigner function of the squeezed Schrödinger-cat state and showed the evolution of the Wigner function in an open system in detail. We estimated the phase in an optical interferometer with the squeezed Schrödinger-cat states (including the squeezed even coherent state, squeezed odd coherent state, and squeezed Yurke-Stoler coherent state). We found that in the limit of a large photon number, the quantum Fisher information can all reach the Heisenberg limit. In particular, the QFI for the SECS can have an order of magnitude factor improvement over the HL in the low-photon-number regime, which is important for fragile systems that cannot withstand large photon fluxes.

APPENDIX A: MASTER EQUATION IN THE DISPLACEMENT REPRESENTATION

To remove the linear term of mode c, i.e., $\Omega_3(ce^{-i\phi_3} + c^\dagger e^{i\phi_3})$, of Eq. (1), we perform a displacement transformation on mode c, i.e., $D(\eta)\rho D^\dagger(\eta) = \rho_{\text{dis}}$, with the displacement operator $D(\eta) = \exp(\eta c^\dagger - \eta^* c)$. Then we have

$$\dot{\rho} = \frac{d}{dt}[D^\dagger(\eta)\rho_{\text{dis}}D(\eta)]$$
$$= \dot{D}^\dagger(\eta)\rho_{\text{dis}}D(\eta) + D^\dagger(\eta)\dot{\rho}_{\text{dis}}D(\eta) + D^\dagger(\eta)\rho_{\text{dis}}\dot{D}(\eta)$$

$$= -i[H, D^\dagger(\eta)\rho_{\text{dis}}D(\eta)] + \kappa_a \mathcal{L}[a, D^\dagger(\eta)\rho_{\text{dis}}D(\eta)]$$
$$+ \kappa_b \mathcal{L}'[b, D^\dagger(\eta)\rho_{\text{dis}}D(\eta)] + \kappa_c \mathcal{L}'[c, D^\dagger(\eta)\rho_{\text{dis}}D(\eta)], \tag{A1}$$

so

$$D^\dagger(\eta)\dot{\rho}_{\text{dis}}D(\eta) = -[\dot{D}^\dagger(\eta)\rho_{\text{dis}}D(\eta) + D^\dagger(\eta)\rho_{\text{dis}}\dot{D}(\eta)]$$
$$- i[H, D^\dagger(\eta)\rho_{\text{dis}}D(\eta)]$$
$$+ \kappa_a \mathcal{L}[a, D^\dagger(\eta)\rho_{\text{dis}}D(\eta)]$$
$$+ \kappa_b \mathcal{L}'[b, D^\dagger(\eta)\rho_{\text{dis}}D(\eta)]$$
$$+ \kappa_c \mathcal{L}'[c, D^\dagger(\eta)\rho_{\text{dis}}D(\eta)]. \tag{A2}$$

After some tedious calculations, one can get the master equation in the displacement representation, i.e., Eq. (6),

$$\frac{d}{dt}\rho_{\text{dis}} = -i[H_{\text{dis}}, \rho_{\text{dis}}] + \kappa_a \mathcal{L}(a, \rho_{\text{dis}}) + \kappa_b \mathcal{L}'(b, \rho_{\text{dis}})$$
$$+ \kappa_c \mathcal{L}'(c, \rho_{\text{dis}}), \tag{A3}$$

by multiplying $D(\eta)$ on the left-hand side and $D^\dagger(\eta)$ on the right-hand side of Eq. (A2) and eliminating the linear terms in the transformed Liouvillian. This process leads to the equation for the amplitude η,

$$\dot{\eta} = -(i\Delta_c + \kappa_c/2)\eta + i\Omega_3 e^{i\phi_3}. \tag{A4}$$

Then its steady value is $\eta_s = \Omega_3 e^{i\phi_3}/(\Delta_c - i\kappa_c/2)$.

APPENDIX B: MASTER EQUATION IN THE SQUEEZED REPRESENTATION

To remove the quadratic term of mode a, i.e., $\Omega_1(a^2 e^{-i\phi_1} + a^{\dagger 2}e^{i\phi_1})$, of Eq. (6), we perform a squeezing transformation on mode a, i.e., $S(\zeta)\rho_{\text{dis}}S^\dagger(\zeta) = \rho_{\text{sq}}$, with the squeeze operator $S(\zeta) = \exp[(\zeta a^{\dagger 2} - \zeta^* a^2)/2]$. Similar to the above displacement transformation, one can get the master equation in the squeezed representation, i.e., Eq. (7),

$$\frac{d}{dt}\rho_{\text{sq}} = -i[H_{\text{sq}}, \rho_{\text{sq}}] + \kappa_a \mathcal{L}(a, \rho_{\text{sq}}) + \kappa_b \mathcal{L}'(b, \rho_{\text{sq}})$$
$$+ \kappa_c \mathcal{L}'(c, \rho_{\text{sq}}) \tag{B1}$$

by eliminating the nondiagonal term of the transformed Hamiltonian, which leads to the equation for the amplitude r,

$$\Delta_a \sinh(2r)/2 - \cosh(2r)\Omega_1 = 0. \tag{B2}$$

Then we have $r = \frac{1}{4}\ln[(\Delta_a + 2\Omega_1)/(\Delta_a - 2\Omega_1)]$.

[1] E. Schrödinger, Die gegenwärtige situation in der quantenmechanik, Naturwissenschaften **23**, 807 (1935).

[2] B. C. Sanders, Review of entangled coherent states, J. Phys. A: Math. Theor. **45**, 244002 (2012).

[3] M. O. Scully and M. S. Zubairy, *Quantum Optics* (Cambridge University Press, Cambridge, 1997).

[4] S. Mancini, V. I. Man'ko, and P. Tombesi, Ponderomotive control of quantum macroscopic coherence, Phys. Rev. A **55**, 3042 (1997).

[5] S. Bose, K. Jacobs, and P. L. Knight, Preparation of nonclassical states in cavities with a moving mirror, Phys. Rev. A **56**, 4175 (1997).

[6] J. Q. Liao and L. Tian, Macroscopic Quantum Superposition in Cavity Optomechanics, Phys. Rev. Lett. **116**, 163602 (2016).

[7] C. C. Gerry and P. L. Knight, Quantum superpositions and Schrödinger cat states in quantum optics, Am. J. Phys. **65**, 964 (1997).

[8] L. Davidovich, M. Brune, J. M. Raimond, and S. Haroche, Mesoscopic quantum coherences in cavity QED: Preparation and decoherence monitoring schemes, Phys. Rev. A **53**, 1295 (1996).

[9] S. Deleglise, I. Dotsenko, C. Sayrin, J. Bernu, M. Brune, J. M. Raimond, and S. Haroche, Reconstruction of non-classical cavity field states with snapshots of their decoherence, Nature (London) **455**, 510 (2008).

[10] W. Ge and M. S. Zubairy, Macroscopic optomechanical superposition via periodic qubit flipping, Phys. Rev. A **91**, 013842 (2015).

[11] Y. Xu, Y. Ma, W. Cai, X. Mu, W. Dai, W. Wang, L. Hu, X. Li, J. Han, H. Wang, Y. P. Song, Z. B. Yang, S. B. Zheng, and L. Sun, Demonstration of Controlled-Phase Gates between Two Error-Correctable Photonic Qubits, Phys. Rev. Lett. **124**, 120501 (2020).

[12] Y. H. Chen, W. Qin, X. Wang, A. Miranowicz, and F. Nori, Shortcuts to Adiabaticity for the Quantum Rabi Model: Efficient Generation of Giant Entangled Cat States via Parametric Amplification, Phys. Rev. Lett. **126**, 023602 (2021).

[13] C. C. Gerry III and E. E. Hach III, Generation of even and odd coherent states in a competitive two-photon process, Phys. Lett. A **174**, 185 (1993).

[14] L. Gilles, B. M. Garraway, and P. L. Knight, Generation of nonclassical light by dissipative two-photon processes, Phys. Rev. A **49**, 2785 (1994).

[15] R. I. Karasik, K. P. Marzlin, B. C. Sanders, and K. B. Whaley, Criteria for dynamically stable decoherence-free subspaces and incoherently generated coherences, Phys. Rev. A **77**, 052301 (2008).

[16] H. Tan, F. Bariani, G. Li, and P. Meystre, Generation of macroscopic quantum superpositions of optomechanical oscillators by dissipation, Phys. Rev. A **88**, 023817 (2013).

[17] M. Mirrahimi, Z. Leghtas, V. V. Albert, S. Touzard, R. J. Schoelkopf, L. Jiang, and M. H. Devoret, Dynamically protected cat-qubits: A new paradigm for universal quantum computation, New J. Phys. **16**, 045014 (2014).

[18] M. J. Everitt, T. P. Spiller, G. J Milburn, R. D. Wilson, and A. M. Zagoskin, Engineering dissipative channels for realizing Schrödinger cats in SQUIDs, Front. ICT **1**, 1 (2014).

[19] Z. Leghtas, S. Touzard, I. M. Pop, A. Kou, B. Vlastakis, A. Petrenko, K. M. Sliwa, A. Narla, S. Shankar, M. J. Hatridge, M. Reagor, L. Frunzio, R. J. Schoelkopf, M. Mirrahimi, and M. H. Devoret, Confining the state of light to a quantum manifold by engineered two-photon loss, Science **347**, 853 (2015).

[20] S. Touzard, A. Grimm, Z. Leghtas, S. O. Mundhada, P. Reinhold, C. Axline, M. Reagor, K. Chou, J. Blumoff, K. M. Sliwa, S. Shankar, L. Frunzio, R. J. Schoelkopf, M. Mirrahimi, and M. H. Devoret, Coherent Oscillations inside a Quantum Manifold Stabilized by Dissipation, Phys. Rev. X **8**, 021005 (2018).

[21] R. Lescanne, M. Villiers, T. Peronnin, A. Sarlette, M. Delbecq, B. Huard, T. Kontos, M. Mirrahimi, and Z. Leghtas, Exponential suppression of bit-flips in a qubit encoded in an oscillator, Nat. Phys. **16**, 509 (2020).

[22] A. Grimm, N. E. Frattini, S. Puri, S. O. Mundhada, S. Touzard, M. Mirrahimi, S. M. Girvin, S. Shankar, and M. H. Devoret, Stabilization and operation of a Kerr-cat qubit, Nature (London) **584**, 205 (2020).

[23] W. Qin, A. Miranowicz, H. Jing, and F. Nori, Generating Long-Lived Macroscopically Distinct Superposition States in Atomic Ensembles, Phys. Rev. Lett. **127**, 093602 (2021).

[24] T. C. Ralph, A. Gilchrist, G. J. Milburn, W. J. Munro, and S. Glancy, Quantum computation with optical coherent states, Phys. Rev. A **68**, 042319 (2003).

[25] J. Gribbin, *Computing with Quantum Cats: From Colossus to Qubits* (Prometheus Books, New York, 2014).

[26] N. Ofek, A. Petrenko, R. Heeres, P. Reinhold, Z. Leghtas, B. Vlastakis, Y. Liu, L. Frunzio, S. M. Girvin, L. Jiang, M. Mirrahimi, M. H. Devoret, and R. J. Schoelkopf, Extending the lifetime of a quantum bit with error correction in superconducting circuits, Nature (London) **536**, 441 (2016).

[27] W. Cai, Y. Ma, W. Wang, C. L. Zou, and L. Sun, Bosonic quantum error correction codes in superconducting quantum circuits, Fund. Res. **1**, 50 (2021).

[28] M. Kira, S. W. Koch, R. P. Smith, A. E. Hunter, and S. T. Cundiff, Quantum spectroscopy with Schrödinger-cat states, Nat. Phys. **7**, 799 (2011).

[29] J. Cheng, Quantum metrology for simultaneously estimating the linear and nonlinear phase shifts, Phys. Rev. A **90**, 063838 (2014).

[30] L. Pezzè, A. Smerzi, M. K. Oberthaler, R. Schmied, and P. Treutlein, Quantum metrology with nonclassical states of atomic ensembles, Rev. Mod. Phys. **90**, 035005 (2018).

[31] B. M. Terhal, Quantum error correction for quantum memories, Rev. Mod. Phys. **87**, 307 (2015).

[32] F. Gaitan, *Quantum Error Correction and Fault Tolerant Quantum Computing* (CRC, Boca Raton, 2008).

[33] *Quantum Error Correction*, edited by D. A. Lidar and T. A. Brun (Cambridge University Press, New York, 2013).

[34] Y. H. Chen, W. Qin, R. Stassi, X. Wang, and F. Nori, Fast binomial-code holonomic quantum computation with ultrastrong light-matter coupling, Phys. Rev. Res. **3**, 033275 (2021).

[35] Y. H. Kang, Y. H. Chen, X. Wang, J. Song, Y. Xia, A. Miranowicz, S. B. Zheng, and F. Nori, Phys. Rev. Res. **4**, 013233 (2022).

[36] J. Sahota and N. Quesada, Quantum correlations in optical metrology: Heisenberg-limited phase estimation without mode entanglement, Phys. Rev. A **91**, 013808 (2015).

[37] H. Lee, P. Kok, and J. P. Dowling, A quantum Rosetta stone for interferometry, J. Mod. Opt. **49**, 2325 (2002).

[38] P. A. Knott, T. J. Proctor, A. J. Hayes, J. P. Cooling, and J. A. Dunningham, Practical quantum metrology with large precision gains in the low-photon-number regime, Phys. Rev. A **93**, 033859 (2016).

[39] L. Shao, W. Li, and X. Wang, Optimal quantum phase estimation in an atomic gyroscope based on a Bose-Hubbard model, Opt. Express **28**, 32556 (2020).

[40] D. S. Schlegel, F. Minganti, and V. Savona, Quantum error correction using squeezed Schrödinger cat states, Phys. Rev. A **106**, 022431 (2022).

[41] A. Ourjoumtsev, H. Jeong, R. Tualle-Brouri, and P. Grangier, Generation of optical 'Schrödinger cats' from photon number states Nature (London) **448**, 784 (2007).

[42] J. Etesse, M. Bouillard, B. Kanseri, and R. Tualle-Brouri, Experimental Generation of Squeezed Cat States with an Operation Allowing Iterative Growth, Phys. Rev. Lett. **114**, 193602 (2015).

[43] K. Huang, H. Le Jeannic, J. Ruaudel, V. B. Verma, M. D. Shaw, F. Marsili, S. W. Nam, E. Wu, H. Zeng, Y.-C. Jeong, R. Filip, O. Morin, and J. Laurat, Optical Synthesis of Large-Amplitude Squeezed Coherent-State Superpositions with Minimal Resources, Phys. Rev. Lett. **115**, 023602 (2015).

[44] X. Y. Lü, G. L. Zhu, L. L. Zheng, and Y. Wu, Entanglement and quantum superposition induced by a single photon, Phys. Rev. A **97**, 033807 (2018).

[45] G. J. Milburn, Quantum Optical Fredkin Gate, Phys. Rev. Lett. **62**, 2124 (1989).

[46] R. B. Patel, J. Ho, F. Ferreyrol, T. C. Ralph, and G. J. Pryde, A quantum Fredkin gate, Sci. Adv. **2**, e1501531 (2016).

[47] Y. Y. Gao, B. J. Lester, K. S. Chou, L. Frunzio, M. H. Devoret, L. Jiang, S. M. Girvin, and R. J. Schoelkopf, Entanglement of bosonic modes through an engineered exchange interaction, Nature (London) **566**, 509 (2019).

[48] X. L. Yin, Y. H. Zhou, and J. Q. Liao, All-optical quantum simulation of ultrastrong optomechanics, Phys. Rev. A **105**, 013504 (2022).

[49] X. Y. Lü, Y. Wu, J. R. Johansson, H. Jing, J. Zhang, and F. Nori, Squeezed Optomechanics with Phase-Matched Amplification and Dissipation, Phys. Rev. Lett. **114**, 093602 (2015).

[50] L. Tang, J. Tang, M. Chen, F. Nori, M. Xiao, and K. Xia, Quantum Squeezing Induced Optical Nonreciprocity, Phys. Rev. Lett. **128**, 083604 (2022).

[51] Z. C. Zhang, Y. P. Wang, Y. F. Yu, and Z. M. Zhang, Quantum squeezing in a modulated optomechanical system, Opt. Express **26**, 11915 (2018).

[52] Z. Zhang and X. Wang, Photon-assisted entanglement and squeezing generation and decoherence suppression via a quadratic optomechanical coupling, Opt. Express **28**, 2732 (2020).

[53] Z. Zhang, L. Shao, W. Lu, Y. Su, Y. P. Wang, J. Liu, and X. Wang, Single-photon-triggered spin squeezing with decoherence reduction in optomechanics via phase matching, Phys. Rev. A **104**, 053517 (2021).

[54] J. R. Johansson, P. D. Nation, and F. Nori, QuTiP: An open source Python framework for the dynamics of open quantum systems, Comput. Phys. Commun. **183**, 1760 (2012).

[55] J. R. Johansson, P. D. Nation, and F. Nori, QuTiP 2: A Python framework for the dynamics of open quantum systems, Comput. Phys. Commun. **184**, 1234 (2013).

[56] U. Leonhardt, *Measuring the Quantum State of Light* (Cambridge University Press, Cambridge, 1997).

[57] S. Ast, M. Mehmet, and R. Schnabel, High-bandwidth squeezed light at 1550 nm from a compact monolithic PPKTP cavity, Opt. Express **21**, 13572 (2013).

[58] K. W. Murch, S. J. Weber, K. M. Beck, E. Ginossar, and I. Siddiqi, Reduction of the radiative decay of atomic coherence in squeezed vacuum. Nature (London) **499**, 62 (2013).

[59] S. Haroche and J. M. Raimond, *Exploring the Quantum: Atoms, Cavities, and Photons* (Oxford University Press, New York, 2006).

[60] M. Aspelmeyer, T. J. Kippenberg, and F. Marquardt, Cavity optomechanics, Rev. Mod. Phys. **86**, 1391 (2014).

[61] M. Jarzyna and R. Demkowicz-Dobrzanski, Quantum interferometry with and without an external phase reference, Phys. Rev. A **85**, 011801(R) (2012).

[62] J. Liu, H. Yuan, X. M. Lu, and X. Wang, Quantum Fisher information matrix and multiparameter estimation, J. Phys. A: Math. Theor. **53**, 023001 (2020).

[63] J. Liu, M. Zhang, H. Chen, L. Wang, and H. Yuan, Optimal scheme for quantum metrology, Adv. Quantum Technol. **5**, 2100080 (2022).

[64] J. Liu, X. X. Jing, and X. Wang, Quantum metrology with unitary parametrization processes, Sci. Rep. **5**, 8565 (2015).

[65] F. Wolfgramm, C. Vitelli, F. A. Beduini, N. Godbout, and M. W. Mitchell, Entanglement-enhanced probing of a delicate material system, Nat. Photon. **7**, 28 (2013).

[66] M. K. Tey, Z. Chen, S. A. Aljunid, B. Chng, F. Huber, G. Maslennikov, and C. Kurtsiefer, Strong interaction between light and a single trapped atom without the need for a cavity, Nat. Phys. **4**, 924 (2008).

[67] M. Pototschnig, Y. Chassagneux, J. Hwang, G. Zumofen, A. Renn, and V. Sandoghdar, Controlling the Phase of a Light Beam with a Single Molecule, Phys. Rev. Lett. **107**, 063001 (2011).

[68] M. A. Taylor, J. Janousek, V. Daria, J. Knittel, B. Hage, H.-A. Bachor, and W. P. Bowen, Biological measurement beyond the quantum limit, Nat. Photon. **7**, 229 (2013).